Barrier-Free Paths of Directed Protein Motion in the Erythrocyte Plasma Membrane

David H. Boal and Seng K. Boey
Department of Physics, Simon Fraser University, Burnaby, British Columbia V5A 1S6, Canada

ABSTRACT A model is presented for the steric interaction between a plasma membrane protein and the membrane cytoskeleton in the human erythrocyte. The cytoskeleton is treated as a network of polymer chains attached to a flat bilayer, and the membrane protein is a hemisphere of effective radius R_e with center on the bilayer edge. The simulation is used to investigate the barrier-free path L for linear guided motion of a protein in the bilayer plane. It is shown that the barrier-free paths of small proteins can be used to extract the effective in-plane diameter of cytoskeletal components. For example, the in-plane diameter of an ankyrin attachment site is found to be approximately 12 nm in the simulation, or twice the computational spectrin diameter. The barrier-free paths of large proteins ($R_e > 23$ nm) vanish when the proteins are corralled by the cytoskeleton. For intermediate size proteins, L decreases approximately as $L \propto S^{-1.4}$ where S is proportional to the sum of the protein and cytoskeleton chain radii.

INTRODUCTION

The lateral diffusion of proteins in a fluid membrane is an important protein transport mechanism. However, the lateral motion of integral membrane proteins is constrained compared with the movement of the constituent lipids of the membrane (Axelrod, 1983; Jacobson et al., 1987). Restricted protein motion is manifested in several different types of experiment. For example, many measurements of the lateral diffusion constant are based upon fluorescence recovery after photobleaching (FRAP). Such measurements yield diffusion constants for integral membrane proteins that may be close to two orders of magnitude smaller than the diffusion constants of membrane lipids or rhodopsin, depending on the protein and cell under investigation (Poo and Cone, 1974; Saffman and Delbrück, 1975; Sheetz et al., 1980; Jacobson et al., 1982; Webb et al., 1982; for a review, see Zhang et al., 1993). For example, Sheetz et al. (1980) find that membrane proteins diffuse approximately 50 times slower in normal mouse erythrocytes than in spherocytic erythrocytes, which lack the major components of the normal erythrocyte membrane matrix. FRAP measurements also show that lateral diffusion constants of proteins are larger when the protein is reconstituted into a pure lipid bilayer than when the same protein is in a membrane with an associated cytoskeleton.

Evidence for restricted motion is also found in single particle tracking (SPT) experiments. Whereas the FRAP technique averages over the motion of many protein molecules, SPT follows the motion of individually labeled proteins (Gross and Webb, 1986; de Brabander et al., 1991; Lee et al., 1991; Tsuda et al., 1992; Kusumi et al., 1993; Ghosh and Webb, 1994; Sako and Kusumi, 1994). Several different modes of protein movement are observed in SPT, ranging from diffusion to highly constrained motion within a corral. The corrals presumably arise from steric interactions with the membrane cytoskeleton.

Recently, the linear guided motion of individually labeled proteins has been used to probe the effects of the cytoskeleton on lateral movement. In the experiments, a latex or gold particle attached to a membrane protein is moved across the plasma membrane in a straight line by optical tweezers (Edidin et al., 1991; Sako and Kusumi, 1995). At some point, the tagged protein encounters a barrier and cannot be held by the force of the tweezers. A barrier-free path (BFP) can be obtained from the mean path length, or from the path length distributions, of the protein motion guided by the optical trap. The BFPs found for two different proteins in the plasma membrane of murine HEPA-OVA cells are in the micron range (Edidin et al., 1991), whereas those of tagged transferrin receptors in rat kidney fibroblastic cells are hundreds of nanometers in length (Sako and Kusumi, 1995).

There are many factors that may affect the diffusion of proteins in the plasma membrane including the steric interaction with the cytoskeleton and in-plane proteins as well as the attraction to other membrane components. Because of viscous and hydrodynamic effects, quantitative theoretical analysis of the FRAP and SPT results is a challenge. Thus far, theoretical models have examined the general properties of particle diffusion through barriers, rather than predicted a diffusion constant for a specific cell/protein system (Saxton, 1982, 1994a,b; Pink, 1985). From a theoretician's point of view, BFPs are unaffected by many dynamical attributes of the cytoskeleton, and so are easier to investigate than diffusion constants.

In this paper, we use a model for the erythrocyte cytoskeleton to predict the BFP as a function of protein size. The choice of the human erythrocyte for our simulations is motivated by the availability of experimental studies on its

Received for publication 9 February 1995 and in final form 11 May 1995.
Address reprint requests to Dr. David H. Boal, Department of Physics, Simon Fraser University, Burnaby, BC V5A 1S6, Canada. Tel.:604-291-5765; Fax: 604-291-3592; E-mail: boal@sfu.ca.

0006-3495/95/08/372/08 $2.00

elastic and geometrical characteristics that can be used to test the simulation. Here, we concentrate on the constraining effects of the cytoskeleton, as opposed to the excluded volume effects of unconstrained in-plane obstacles for two reasons: (i) Some proteins show a much smaller diffusion constant when measured in a cell with a membrane-associated cytoskeleton than when measured in an artificial vesicle without a cytoskeleton (see Sheetz et al., 1980, as well as Zhang et al., 1993). (ii) Studies of model membranes show that the diffusion constant is reduced by only a factor of five as the protein concentrations in the model bilayer is increased from 0% to 50% (Pink, 1985). However, experimental measurements show that the reduction in the presence of a cytoskeleton may be close to two orders of magnitude.

In other words, although the presence of proteins in the bilayer undoubtedly reduces the diffusion constant, the reduction caused by the cytoskeleton may be just as large, if not larger.

The purpose of this paper is twofold. First, we investigate the interpretation of observables that can be extracted from the BFP measurements by using a computational cytoskeleton with known geometry. Second, we make specific predictions for the human erythrocyte by setting the length scale of the simulation using a number of independent measurements.

The simulation of directed protein motion in the human erythrocyte is described in the following section. We then outline the methodology for extracting the BFP in the simulation. Two regimes of BFP are investigated in some detail. It is demonstrated that the effective in-plane sizes of some cytoskeletal components can be determined from the BFPs of small proteins. This method is probably of more general utility than the task to which it is placed here. It is also shown that large proteins are corralled by the cytoskeleton. The corral size observed in the simulation is in the range expected from the cytoskeleton geometry. Finally, the Appendix summarizes the elastic properties predicted by the simulation for the human erythrocyte cytoskeleton, and these are used as a check on the descriptive accuracy of the model cytoskeleton.

SIMULATION

The computational model that we use for the erythrocyte cytoskeleton is based on one that has been used to predict the cytoskeleton elastic and geometrical properties (Boal, 1994). In the model, each spectrin tetramer is represented by a single polymer chain with n_{seg} segments and the chains are linked together at sixfold coordinate junction vertices. Thus, the vertices that make up the chain are twofold coordinate, except at the junction complexes where they are sixfold coordinate. The chain midpoints are forced to lie in the computational xy plane representing the bilayer, although they are free to move throughout the xy plane. With the exception of the midpoints, all chain elements are restricted to lie in the positive z direction that represents the cytoplasmic side of the bilayer. The junction vertices represent the actin junctions of the cytoskeletal network, whereas the binding of the chain midpoints to the xy plane mimics the ankyrin attachment of the cytoskeleton to the lipid bilayer.

Experiment may ultimately show that both the tetramer midpoints and the junction complexes are attached to proteins resident in the bilayer plane. Only the tetramer midpoints are attached to the bilayer in the current model. However, the junction vertices in the simulation are not far removed from the bilayer plane: the network has a thickness of 16 nm (see below).

In our original investigation of the cytoskeleton elastic properties (Boal, 1994), the polymer chains were modeled by bead-and-tether interactions, which is efficient for Monte Carlo simulation. Because we are ultimately interested in studying dynamical quantities such as diffusion coefficients, the simulation of this paper is based on molecular dynamics, which requires a smoother interparticle potential than the square-well interaction of hard beads and tethers. We use a potential developed by Bishop, Kalos, and Frisch (BKF hereafter; Bishop et al., 1979) for polymer studies, in which any two vertices are subject to a short-range repulsive interaction

$$V_{rep}(r) = 4\varepsilon\{(\sigma/r)^{12} - (\sigma/r)^6 + 1/4\} \qquad 0 < r < 2^{1/6}\sigma$$
$$= 0 \qquad r > 2^{1/6}\sigma, \tag{1}$$

where ϵ and σ are the fundamental energy and length scales of the simulation and r is the distance between the vertices. A nearest neighbor potential V_{nn} provides the interaction that holds the network together; each vertex is connected to either two (along the chain) or six (at chain junctions) neighboring vertices through

$$V_{nn}(r) = -0.5kR_c^2 \ln[1 - (r/R_c)^2], \tag{2}$$

where k and R_c are parameters. We use the dimensionless parameter set $R_c/\sigma = 1.5$ and $k\sigma^2/\epsilon = 30$ (Grest and Kremer, 1986). The positions of the vertices are evolved by molecular dynamics using a simple leapfrog algorithm to integrate the equations of motion with time step $\Delta t = 0.005\,(m\sigma^2/\epsilon)^{1/2}$, where m is the vertex mass. The observables of interest in this paper, such as the BFPs, elastic constants, and membrane areas, depend only on the temperature and σ. Fixing values for σ and the temperature allows us to convert the results of the simulation to physical units, and this is done later in the paper. The investigation of time-dependent quantities such as diffusion constants would require a more detailed simulation of the spectrin tetramers, including viscous effects, to determine the parameters m and ϵ.

The simulation is performed at constant temperature and pressure with periodic boundary conditions in the x and y directions. In an isobaric ensemble, the lengths L_x and L_y of the rectangular boundary are allowed to fluctuate. The fluctuations in L_x and L_y are obtained from a Monte Carlo algorithm developed by Wood (1968; see also Hansen and

McDonald, 1986). The implementation of the technique in this cytoskeleton model can be found elsewhere (Boal, 1994). In essence, attempts are made to change the box lengths L_x and L_y by random amounts, and the changes are accepted according to a Boltzmann weight. The simulations reported here are performed at zero pressure.

The number of segments n_{seg} is a parameter of the simulation, fixed by the properties of the human erythrocyte cytoskeleton. Physically, it is equal to the effective number of segments in a spectrin tetramer. The combined potential of Eqs. 1 and 2 has a minimal energy at a segment length of 0.97σ. Hence, at low temperature the contour length along a single chain with n_{seg} segments is approximately $0.97n_{seg}\sigma$. However, the average end-to-end displacement is much shorter than the contour length, as one knows from the behavior of random walks. Thus, the average area of the network in the xy plane, $\langle A\rangle$, is smaller than what its "stretched" size A_s would be if all the chains were straight and of length $0.97n_{seg}\sigma$. Computationally, the equilibrium area as a function of n_{seg} is found to be

$$A_s/\langle A\rangle = 0.43n_{seg}^{0.8}. \tag{3}$$

The experimentally observed ratio of the stretched to equilibrium area, seven (see Steck, 1989), allows us to fix n_{seg} at 32 according to Eq. 3. The physical value for σ is not determined by this area ratio, but rather by the contour length of the spectrin tetramers.

In the simulation, the chains are only attached to the bilayer plane at the chain midpoints, which results in the network having a finite thickness. For a single configuration, the thickness t is defined as the average value of the vertex heights above the computational xy plane representing the bilayer. The ensemble average value of t is found to be

$$\langle t\rangle/\sigma = 0.11n_{seg}^{0.9}. \tag{4}$$

For $n_{seg} = 32$ and $\sigma = 6.4$ nm, the erythrocyte cytoskeleton is predicted to have a thickness $\langle t\rangle$ of 16 nm. The scaling behavior of both $\langle A\rangle$ and $\langle t\rangle$ as a function of n_{seg} is similar to what was found in our previous study of the erythrocyte cytoskeleton using square-well potentials (Boal, 1994).

The model cytoskeleton is allowed to relax for several million Monte Carlo steps before an attempt is made to choose a sample network configuration (called a realization) for investigation. Once the network has relaxed, its in-plane area fluctuates around an equilibrium value of $A_s/\langle A\rangle = 6.9$ for $n_{seg} = 32$. To fix σ at the physical length scale, one particular realization is chosen with A_s/A within 1% of the equilibrium value. An alternate, but more memory-intensive, procedure would be to average over many realizations. However, we feel that a single realization with 64 junction vertices is sufficiently large that it properly represents the geometrical properties of the network.

To evaluate the BFP, a computational protein is introduced in the model cytoskeleton prepared as described above. Of the many possible shapes that could be used for the protein, we choose a sphere whose center is on the xy plane. Because the xy plane represents the bilayer edge, then our choice of geometry corresponds to the protein having a spherical shape in the cytoplasm. The interaction between the protein and the cytoskeleton elements is taken to be of similar form to Eq. 1,

$$V_{pro}(r) = 4\varepsilon\{(S/r)^{12} - (S/r)^6 + 1/4\} \qquad 0 < r < 2^{1/6}S$$
$$= 0 \qquad r > 2^{1/6}S, \tag{5}$$

where S is a variable reflecting the length scale of the protein-spectrin interaction. Although this potential does not have a hard-core radius, it does increase rapidly for r not much less than S. We define an effective protein radius later in this paper by subtracting out the contribution of the spectrin radius to S.

The computational protein is introduced into the bilayer plane at a random point and is moved in a straight line through the network in a randomly chosen direction. This aspect of the simulation is similar to the guided protein motion in the optical trap experiments (Edidin et al., 1991; Sako and Kusumi, 1995). In the simulation, the protein trajectory is advanced in small steps (0.001σ), and at each step the force on the protein arising from the cytoskeleton via Eq. 5 is evaluated. Once the force from the cytoskeleton exceeds a predetermined threshold value F_o, the protein is deemed to have escaped from the trap and the displacement of the protein from the start of its trajectory is stored. A total of 100,000 trajectories is generated for each value of S and F_o.

Fig. 1 shows a view of the network from the $+z$ direction (cytoplasmic side). The shaded lines indicate the position of the cytoskeleton, with elements nearer the viewer indicated by lighter shading. The stopping points of proteins with $S/\sigma = 0.89$ are shown as white disks, of diameter 0.89σ. One can see that a large number of the stopping points occur at the chain midpoints, where the chains are attached to the computational bilayer. The choice $S/\sigma = 0.89$ corresponds to the protein having the same effective radius as the effective radius of the spectrin.

BARRIER-FREE PATH

We use the following method to extract the BFP in the simulation. For each combination of the protein radius parameter S and the trapping force F_o, a total of 100,000 protein trajectories are collected. Each straight-line trajectory has an end-to-end path length d. From the distribution of these path lengths $P(d)$, we extract a mean path λ. Even at fixed protein radius, the mean path depends upon the trapping force. We define the BFP L as the value of λ obtained in the zero-force limit.

Because we extract the BFP in the limit where F_o vanishes, we do not expect that it is necessary to include the dynamical evolution of the cytoskeleton as each protein trajectory is generated. Thus, the computational cytoskele-

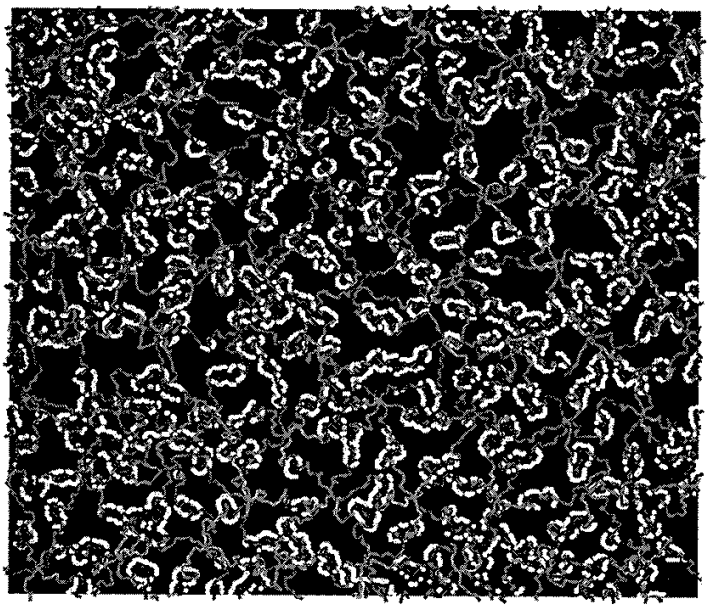

FIGURE 1 Computational network with 64 junction vertices (8 rows of 8 vertices) and $n_{seg} = 32$. In this figure, $S/\sigma = 0.89$ and $F_o\sigma/\epsilon = 0.05$. Chain elements nearer the viewer are drawn with lighter shading. The stopping points of the proteins are indicated by white disks of diameter 0.89σ. A total of 10,000 endpoints are shown.

ton is held fixed while the protein is moved along the bilayer. The dependence of λ on the trapping force in the simulation is weaker than what may be observed experimentally, as the simulation does not allow the protein dragged by the optical trap to move elements of the cytoskeleton out of its way. Of course, the computational protein may force its way through the static cytoskeleton if F_o is large enough. It would be computationally prohibitive for us to generate a large sample of protein trajectories if it were necessary to evolve the cytoskeleton at the same time as the trajectories are constructed.

Each straight line trajectory of the computational protein has a path length d. The distribution of path lengths for 100,000 trials at $S/\sigma = 0.89$ and $F_o\sigma/\epsilon = 0.05$ is shown in Fig. 2. The figure is a log-linear plot and clearly shows that the distribution is exponential over much of its range. We fit the distribution $P(d)$ over the exponential range with

$$P(d) \approx \exp(-d/\lambda), \tag{6}$$

where λ is the mean path for the combination of S and F_o chosen. We expect the distribution to be exponential if, in analogy with scattering theory (Segre, 1965), the protein passes through a region of random scattering centers. Later in this paper, λ for small proteins is related to the cross section of the objects that terminate the trajectories.

Because the repulsive potential in Eq. 5 does not have a sharp cutoff radius (as an infinite step-function potential does), then the mean path can increase with F_o. At large F_o, the protein simply is forced through the network. This behavior can be seen in Fig. 3, where λ is given as a function of F_o for three values of S. The mean path monotonically increases with cutoff force for $F_o\sigma/\epsilon > 0.1$ at all values of S investigated. However, the mean path λ depends only weakly on F_o as the guided protein cannot move the cytoskeleton out of its way in the simulation.

If the cutoff force is very small, then a guided protein is stopped as soon as it encounters the cytoskeleton. Thus, we expect that λ should be independent of F_o for small F_o. This behavior is also visible in Fig. 3. In the simulation, we find

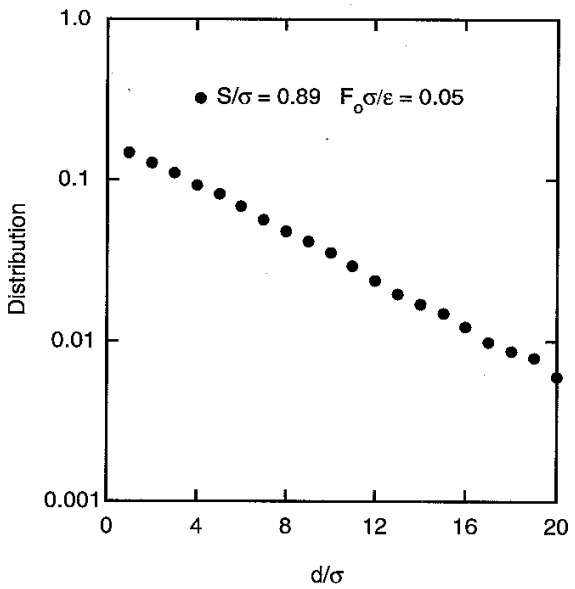

FIGURE 2 Distribution of path lengths d for fixed values of $S/\sigma = 0.89$ and $F_o\sigma/\epsilon = 0.05$. The distribution is constructed from 100,000 paths. The form of the distribution is approximately exponential over much of the range in d.

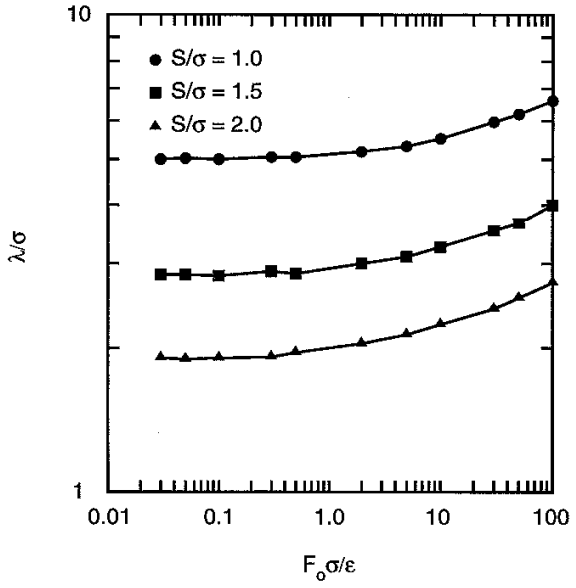

FIGURE 3 Mean path length λ shown as a function of the cutoff force F_o. The transition between force-dependent and force-independent behavior of λ occurs at approximately $F_o\sigma/\epsilon = 0.1$. Three data sets are shown: S/σ = 1.0, 1.5, and 2.0. The line segments are drawn to guide the eye.

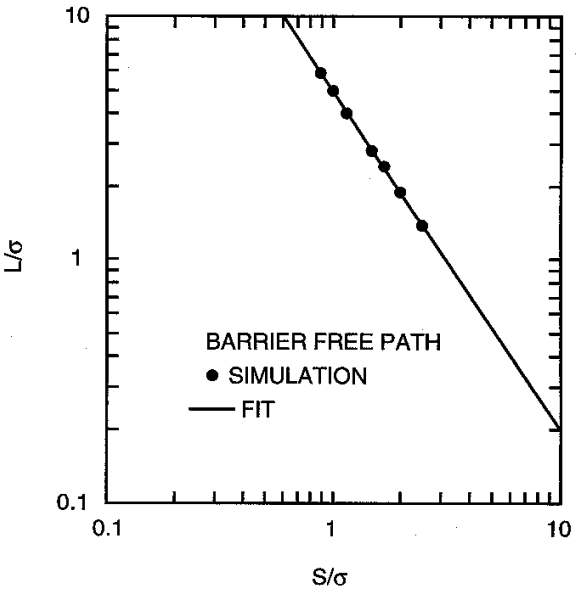

FIGURE 4 Logarithmic plot of BFP L shown as a function of protein size parameter S. The straight line through the data is the fit $L/\sigma = 5.0\ (S/\sigma)^{-1.4}$.

that the change from force-dependent to force-independent λ occurs at approximately $F_o\sigma/\epsilon = 0.1$. Thus, we define the BFP as the asymptotic value of λ which is found for $F_o\sigma/\epsilon \rightarrow 0$. This procedure for extracting L is repeated for several values of protein interaction length parameter S. A summary of the BFPs so determined is given as a function of S in Fig. 4.

We expect that small proteins can move more easily through the cytoskeleton than large proteins can, and this behavior is observed in Fig. 4. The figure illustrates that the decrease in BFP is approximately of power law form:

$$L/\sigma = 5.0(S/\sigma)^{-1.4} \tag{7}$$

for the range of protein sizes investigated. Eq. 7 shows that the BFP vanishes as the protein size parameter S approaches the geometrical length scale of an average spectrin chain. However, the functional form of Eq. 7 will not apply at large S as the cytoskeleton puts a bound on the largest protein that can fit into the spectrin network. That is, the cytoskeleton "corral" forces L to vanish at finite S, and not exclusively in the large S limit implied by Eq. 7.

Before applying the simulation results to the erythrocyte, we change both units and variables. First, the results are translated to nanometers using the spectrin tetramer contour length. Because each spectrin tetramer has a contour length of 200 nm, then the corresponding value of σ must be 6.4 nm if $n_{seg} = 32$. Second, the potential parameter S, which is the sum of both the protein size and cytoskeleton chain thickness, is replaced by a variable with a more transparent geometrical interpretation. The repulsive interaction between different vertices on the cytoskeleton chain vanishes at $2^{1/6}\sigma$, meaning that individual chain elements have a cutoff radius of $\sigma/2^{5/6}$ for their interaction with each other. The cutoff distance for the protein-spectrin interaction is $2^{1/6}S$. We therefore subtract the spectrin radius from S and define an effective protein radius R_e of

$$R_e/\sigma = 2^{1/6}(S/\sigma - 1/2) \tag{8}$$

for the interaction between the membrane protein and the cytoskeleton.

Large proteins measure the corral size

Large proteins have a small BFP, as their motion is highly restricted by steric interactions with the cytoskeleton; that is, the protein cannot pass out of the corral defined by three spectrin tetramers attached in triangular form. For sufficiently large protein radius R_e, each protein trajectory is confined to lie within a single corral. Thus, whereas L should be large for small R_e, it should steadily decrease with increasing R_e. The sum $L + R_e$ should approach a constant value as R_e approaches the largest value allowed by the corral geometry. This behavior is observed in Fig. 5, where $L + R_e$ is plotted against R_e. In Fig. 5, the limiting value of $L + R_e$ is 23 nm.

As a technical note, the figure shows that $L + R_e$ is slightly more than 23 nm for the largest protein sizes (smallest L) investigated. This effect arises because very large proteins cannot fit into some of the corrals, so the config-

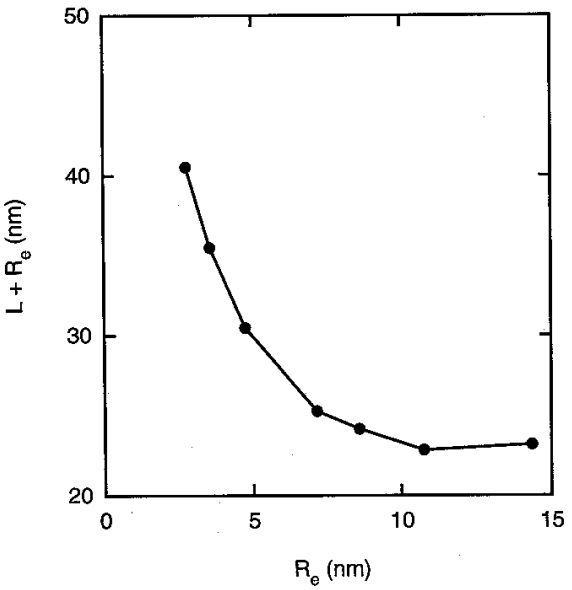

FIGURE 5 $L + R_e$ shown as a function of the effective protein radius R_e. The conversion of simulation units to physical units uses $\sigma = 6.4$ nm. In the large R_e limit, $L + R_e$ has a value of 23 nm. The line segments are drawn to guide the eye.

urations sampled become more heavily weighted by large corrals. In other words, the BFPs of large proteins ($R_e > 2.5\sigma$) are not evaluated with the full configuration space available to small and medium sized proteins.

Is this value for the corral size approximately what we expect from the geometry of the computational cytoskeleton? Consider an equilateral triangle with side length b equal to the average separation between the sixfold junction vertices. The maximal radius of a circle that can be inscribed inside this triangle is $b/(2\sqrt{3})$. If we treat a cytoskeleton corral as an equilateral triangle with $b = 70$ nm (the average separation between junction complexes in the human erythrocyte), then the radius of the inscribed circle is 20 nm. This is close to the upper bound of 23 nm found for the protein effective radius in Fig. 5. In other words, the effective corral radius obtained in the limit of large protein size is a reasonable reflection of the corral geometry.

Small proteins measure the cytoskeleton attachment points

In the simulation, small proteins have large BFPs as their trajectories encounter few obstacles associated with the cytoskeleton. The main component of the computational cytoskeleton that can affect such proteins is the set of attachment points representing the ankyrin junctions. The remainder of the chain network is away from the bilayer plane. The chain midpoints then act as a sequence of barriers that scatter the guided protein as it moves along the computational xy plane representing the bilayer. The exponential distribution of path lengths shown in Fig. 2 supports the interpretation of guided motion of small proteins in terms of two-dimensional scattering.

In classical two-dimensional scattering, the mean free path of a point particle traversing a target of disks (edge-on) is equal to $(\rho D)^{-1}$, where ρ is the area density of scattering centers and D is the disk diameter (see, for example, Segre, 1965). If we treat the BFP of small proteins as a scattering problem, then ρ is the area density of ankyrin attachment points and D is the effective diameter of ankyrin in the bilayer plane. For non-zero R_e, both the protein and ankyrin sizes are included in D. In the simulation, the BFP can be used to extract the size of the ankyrin attachment sites by determining the value of L as $R_e \rightarrow 0$. The limiting value of L^{-1} can be obtained graphically, as shown in Fig. 6. The behavior of L^{-1} is seen to be linear in R_e at small radii, and the zero radius limit of L^{-1} is 8.5×10^{-3} nm^{-1} by extrapolation.

The area density ρ must be known to extract the effective ankyrin diameter from L^{-1} via $\rho D = L^{-1}$. The area density of the ankyrin junctions is $(2\sqrt{3})/b^2$, where b is the average distance between the sixfold junction vertices of the cytoskeleton. Taking b to be 70 nm, then ρ is 7.1×10^{-4} nm^{-2}. This yields $D = 12$ nm if $L^{-1} = 8.5 \times 10^{-3}$ nm^{-1}. For comparison, the cutoff radius for interaction between chain elements is $\sigma/2^{5/6} = 7.2$ nm. Thus, the effective in-plane diameter of the attachment sites is approximately twice the diameter of the chains themselves. Of course, one should not expect these numbers to be identical as D is a

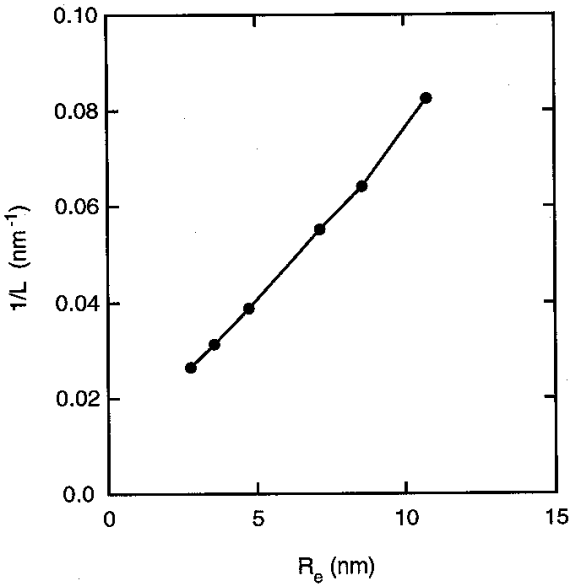

FIGURE 6 Behavior of L^{-1} at small protein effective radius R_e. The same unit conversion is used as in Fig. 5. In the $R_e \rightarrow 0$ limit, L^{-1} has a value of 8.5×10^{-3} nm^{-1}. The line segments are drawn to guide the eye.

TABLE 1 Comparison of the reduced elastic moduli of two model representations of the cytoskeleton

Model	$\beta K_A l^2$	$\beta \mu l^2$	$\beta K_V l^3$	$\beta Y_\perp l^3$
BKF	$192 n_{seg}^{-2.0}$	$81 n_{seg}^{-2.0}$	$2800 n_{seg}^{-3.1}$	$91 n_{seg}^{-0.9}$
Bead and tether	$43 n_{seg}^{-1.7}$	$25 n_{seg}^{-1.7}$	$193 n_{seg}^{-2.4}$	$87 n_{seg}^{-2.0}$

One model is the BKF potential used in this paper, and the other model is the bead-and-tether interaction used in previous work (Boal, 1994). The length scale l is equal to σ in the BKF interaction and a (the bead diameter) in the bead-and-tether interaction. The moduli are shown as a function of n_{seg}. The uncertainty in the exponents is approximately 10%.

quantity that averages over thermal fluctuations of the chain configurations. In conclusion, we see that the BFP of small proteins can be used to extract the effective in-plane diameter of scattering centers such as ankyrin.

SUMMARY

Through computer simulation, we investigate the directed motion of a membrane protein in the plasma membrane of the human erythrocyte. The simulation is used to mimic the motion of proteins dragged by optical tweezers. For each combination of trapping force and protein radius, the distribution of path lengths for this motion is found to be exponential, from which a mean path λ can be extracted. This exponential behavior is expected on general grounds for the scattering of small probes by randomly distributed target objects. For a fixed protein size, the mean path increases with the force of the optical trap. However, λ is relatively constant for weak trapping force, and the BFP L is obtained in the simulation by extrapolating λ to zero trapping force.

For intermediate size proteins, the simulation predicts that L decreases with increasing protein size as $L/\sigma = 5.0\,(S/\sigma)^{-1.4}$, where σ and S are length scales associated with the repulsive potentials within the network chains, and between the protein and the chains, respectively. Of more importance biologically is the relationship between L and R_e, the protein effective radius. At large R_e, the BFP vanishes, corresponding to the protein being corralled by the cytoskeleton. The largest proteins allowed by the average corral are found to have an effective radius of 23 nm, a result consistent with a value of 20 nm expected from network geometry.

Small proteins can be used to determine the effective in-plane diameter of the ankyrin proteins that attach the cytoskeleton to the membrane. The BFP as $R_e \rightarrow 0$ is interpreted in terms of two-dimensional scattering as being equal to $(\rho D)^{-1}$, where ρ is the area density of ankyrin junctions and D is the average diameter of the junction. Both the geometrical size of ankyrin and the effects of thermal fluctuations in the chain geometry are included in D. In the simulation, D is found to be approximately 12 nm, or roughly twice the computational spectrin tetramer diameter. Interpreted in terms of scattering theory, the BFPs of small objects that could be guided through the plasma membrane can provide an in situ measurement of the effective in-plane sizes of some, but not all, cytoskeletal and other elements of the membrane.

TABLE 2 Comparison of the elastic moduli predicted for the human erythrocyte cytoskeleton by the two model interactions in Table 1

Model	K_A(J/m^2)	μ(J/m^2)	K_V(J/m^3)	$Y_\perp$(J/m^3)
BKF	1.8×10^{-5}	7.7×10^{-6}	0.9×10^{3}	6.1×10^{4}
Bead and tether	1.7×10^{-5}	9.6×10^{-6}	1.2×10^{3}	2.0×10^{3}

The parameters for the cytoskeleton are $n_{seg} = 32$ and $l = \sigma = 6.4$ nm in the BKF model and $n_{seg} = 26$ and $l = a = 6.4$ nm in the bead-and-tether model. The predicted moduli have uncertainties of approximately 10%.

APPENDIX

The simulation used in this paper is based on the BKF potential for polymer chains (Bishop et al., 1979) and is different from the bead-and-tether potential used in an earlier study of the erythrocyte cytoskeleton (Boal, 1994). It is important to verify that the elastic properties of both computational networks agree, as the moduli should depend mainly on entropy and network geometry. The elastic moduli of the two models can be extracted by using standard methods (Boal, 1994). The dependence of the network elastic properties on the number of chain segments n_{seg} is summarized in Table 1 for both networks. There are four elastic constants shown: two in-plane constants (the area compression modulus K_A and the in-plane shear modulus μ) and two moduli involving transverse properties of the network (the volume compression modulus K_A and the transverse Young's modulus $Y_\perp$). The power law dependence of the moduli on n_{seg} agrees within statistical uncertainty for both networks, except for the transverse Young's modulus.

According to Table 1, networks using the BKF potential are stiffer in the transverse direction than those using the bead-and-tether potential. This arises from the limited ability of a BKF chain to reverse direction at a vertex. Bead-and-tether chains can reverse direction more easily, as the maximal tether length is significantly larger than the bead diameter. Whereas individual chains in the two models have similar stiffness, the sixfold coordinate junction vertices are significantly more rigid for the BKF potential.

To mimic the geometrical properties of the erythrocyte cytoskeleton, the bead-and-tether network requires the number of segments n_{seg} to be 26, which is smaller than the value of 32 found for the BKF potential. However, this difference is expected as the chain persistence length with the BKF potential is roughly 10% larger than that of the bead-and-tether chains (Boal, 1994). Because the BKF chains are stiffer than the bead-and-tether chains, more segments are needed to effect a given reduction in network area with the BKF potential.

The elastic moduli predicted for the human erythrocyte cytoskeleton are shown in Table 2. With the exception of the transverse Young's modulus, the predicted moduli for the two model networks agree to within 10–20%, which is the statistical uncertainty of the predictions owing to finite sample size. The fact that the predictions of the two models agree is a check on the accuracy of the simulations. A comparison of the predicted elastic moduli with the available experimental measurements is given by Boal (1994).

The authors thank Evan Evans and Ken Jacobson for many stimulating discussions and Akihiro Kusumi for comments provided during the preparation of this manuscript. This work is supported in part by the Natural Sciences and Engineering Research Council of Canada.

REFERENCES

Axelrod, D. 1983. Lateral motion of membrane proteins and biological function. *J. Membr. Biol.* 75:1–10.

Bishop, M., M. H. Kalos, and H. L. Frisch. 1979. Molecular dynamics of polymeric systems. *J. Chem. Phys.* 70:1299–1304.

Boal, D. H. 1994. Computer simulation of a model network for the erythrocyte cytoskeleton. *Biophys. J.* 67:521–529.

de Brabander, M., R. Nuydens, A. Ishihara, B. Holifield, K. Jacobson, and H. Geerts. 1991. Lateral diffusion and retrograde movements of individual cell surface components on single motile cells observed with nanovid microscopy. *J. Cell. Biol.* 112:111–124.

Edidin, M., S. C. Kuo, and M. P. Sheetz. 1991. Lateral movements of membrane glycoproteins restricted by dynamic cytoplasmic barriers. *Science*. 254:1379–1382.

Ghosh, R. N., and W. W. Webb. 1994. Automated detection and tracking of individual and clustered cell surface low density lipoprotein receptor molecules. *Biophys. J.* 66:1301–1318.

Gross, D., and W. W. Webb. 1986. Molecular counting of low-density lipoprotein particles as individuals and small clusters on cell surfaces. *Biophys. J.* 49:901–911.

Grest, G. S., and K. Kremer. 1986. Molecular dynamics simulation for polymers in the presence of a heat bath. *Phys. Rev.* A33:3628–3631.

Hansen, J. P., and I. R. McDonald. 1986. Theory of Simple Liquids. Academic Press, New York.

Jacobson, K., E. Elson, D. Koppel, and W. W. Webb. 1982. Fluorescence photobleaching in cell biology. *Nature*. 295:283–284.

Jacobson, K., A. Ishihara, and R. Inman. 1987. Lateral diffusion of proteins in membranes. *Annu. Rev. Physiol.* 49:163–175.

Kusumi, A., Y. Sako, and M. Yamamoto. 1993. Confined lateral diffusion of membrane receptors as studied by single particle tracking (nanovid microscopy): effects of calcium-induced differentiation in cultured epithelial cells. *Biophys. J.* 65:2021–2040.

Lee, G. M., A. Ishihara, and K. A. Jacobson. 1991. Direct observation of Brownian motion of lipids in a membrane. *Proc. Natl. Acad. Sci. USA*. 88:6274–6278.

Pink, D. A. 1985. Protein lateral movement in lipid bilayers. Simulation studies of its dependence upon protein concentration. *Biochim. Biophys. Acta*. 818:200–204.

Poo, M.-M., and R. Cone. 1974. Lateral diffusion of rhodopsin in the photoreceptor membrane. *Nature*. 247:438–441.

Saffman, P. G., and M. Delbrück. 1975. Brownian motion in biological membranes. *Proc. Natl. Acad. Sci. USA*. 72:3111–3113.

Sako, Y., and A. Kusumi. 1994. Compartmentalized structure of the plasma membrane for receptor movements as revealed by a nanometer-level motion analysis. *J. Cell Biol.* 125:1251–1264.

Sako, Y., and A. Kusumi. 1995. Barriers for lateral diffusion of transferrin receptors in the plasma membrane as characterized by receptor dragging by laser tweezers: fence *vs.* tether. *J. Cell Biol.* In press.

Saxton, M. 1982. Lateral diffusion in an archipelago: effects of impermeable patches on diffusion in a cell membrane. *Biophys. J.* 39:165–173.

Saxton, M. 1994a. Anomalous diffusion due to obstacles: a Monte Carlo study. *Biophys. J.* 66:394–401.

Saxton, M. 1994b. Single particle tracking: models of directed transport. *Biophys. J.* 67:2110–2119.

Segre, E. 1965. Nuclei and Particles. W. A. Benjamin, New York. Chap. 2. 17–70.

Sheetz, M. P., M. Schindler, and D. E. Koppel. 1980. Lateral mobility of integral membrane proteins is increased in spherocytic erythrocytes. *Nature*. 285:510–512.

Steck, T. L. 1989. Red cell shape. *In* Cell Shape: Determinants, Regulation and Regulatory Role. W. Stein and F. Bronner, editors. Academic Press, New York. 205–246.

Tsuda, K., Y. Sako, and A. Kusumi. 1992. Interaction between integral membrane proteins and the membrane skeleton in human erythrocyte as studied by nanometer-level analysis of movements. *Cell Struct. Funct.* 17:487.

Webb, W. W., L. S. Barak, D. W. Tank, and E. S. Wu. 1982. Molecular mobility on the cell surface. *Biochem. Soc. Symp.* 46:191–205.

Wood, W. W. 1968. Monte Carlo calculations for hard disks in the isothermal-isobaric ensemble. *J. Chem. Phys.* 48:415–434.

Zhang, F., G. M. Lee, and K. Jacobson. 1993. Protein lateral mobility as a reflection of membrane microstructure. *BioEssays*. 15:579–588.